Long-Tailed Characteristic of Spiking Pattern Alternation Induced by Log-Normal Excitatory Synaptic Distribution

Sou Nobukawa, *Member, IEEE*, Haruhiko Nishimura, *Member, IEEE*,
Nobuhiko Wagatsuma, Satoshi Ando, and Teruya Yamanishi

Abstract—Studies of structural connectivity at the synaptic level show that in synaptic connections of the cerebral cortex, the excitatory postsynaptic potential (EPSP) in most synapses exhibits sub-mV values, while a small number of synapses exhibit large EPSPs ($\gtrsim$ 1.0 [mV]). This means that the distribution of EPSP fits a log-normal distribution. While not restricting structural connectivity, skewed and long-tailed distributions have been widely observed in neural activities, such as the occurrences of spiking rates and the size of a synchronously spiking population. Many studies have been modeled this long-tailed EPSP neural activity distribution; however, its causal factors remain controversial. This study focused on the long-tailed EPSP distributions and interlateral synaptic connections primarily observed in the cortical network structures, thereby having constructed a spiking neural network consistent with these features. Especially, we constructed two coupled modules of spiking neural networks with excitatory and inhibitory neural populations with a log-normal EPSP distribution. We evaluated the spiking activities for different input frequencies and with/without strong synaptic connections. These coupled modules exhibited intermittent intermodule-alternative behavior, given moderate input frequency and the existence of strong synaptic and intermodule connections. Moreover, the power analysis, multiscale entropy analysis, and surrogate data analysis revealed that the long-tailed EPSP distribution and intermodule connections enhanced the complexity of spiking activity at large temporal scales and induced nonlinear dynamics and neural activity that followed the long-tailed distribution.

Index Terms—Log-normal distribution, long-tailed distribution, pattern alternation, spiking neural network.

I. INTRODUCTION

RECENT studies using neuroimaging modalities, such as functional magnetic resonance imaging (fMRI),

electroencephalography (EEG), and magnetoencephalography (MEG), to capture brain activity have elucidated the role of spatiotemporal fluctuations of neural activity in brain function [1]–[6]. Studies using diffusion tensor imaging with high spatial resolution have also revealed the complex brain network structures that produce fluctuations in neural activity [7]–[10]. Especially, the brain network possesses feedback loops at multiple hierarchical levels [11] and with complex characteristics, such as high-degree nodes, high clustering, short path length, and high centrality [12]–[17]. It has previously been suggested that these brain network structures produce the complex activity; accordingly, various models with spiking neural networks have been proposed [18]–[21] (review in [9] and [22]). In particular, Riecke *et al.* [23] and Shanahan [24] demonstrated that the highly complex neural activity is induced by the small worldness of synaptic connections in spiking neural networks.

Moreover, studies of structural connectivity at the synaptic-level show that the excitatory postsynaptic potential (EPSP) of most cerebral synapses exhibits sub-mV values, while a small number of synapses exhibit large EPSPs ($\gtrsim$ 1.0 [mV]), i.e., the distribution of EPSP fits a log-normal distribution [25], [26]. Modeling studies focusing on the log-normal distribution of EPSPs have described spontaneous activity [27], [28], which is fluctuated spiking activity that is sustained even in the absence of external stimulation [20], [29], [30]. Moreover, Kriener *et al.* [31] reported that this spontaneous activity that was induced by the log-normal distribution of EPSPs exhibited a complex behavior with slow temporal transitions between bistable activity states. Recently, Kada *et al.* [32] and Nobukawa *et al.* [33] introduced a spiking neural network with a physiologically observed duality of a complex synaptic connection depending on the magnitude of EPSP. Furthermore, we reproduced the complex spatiotemporal spontaneous activity with multiple states of neural activity [33].

Physiological experimental studies have revealed that fluctuations of neural activity exhibit spatiotemporal behaviors with skewed and long-tailed distributions (reviewed in [9]). In particular, when considering the probability of spiking rates [34]–[40] and the size of synchronously spiking populations [35], [41], a log-normal distribution is exhibited. In visual perception, when an ambiguous figure with two different interpretations is presented, the period of dominant perception (which involves unilateral stimuli interpretation)

follows a heavy-tailed, unimodal, maximum peak distribution, such as that of gamma or log-normal distribution [42]–[45] (reviewed in [46]). In a modeling study of the long-tailed distribution of neural activity, Kossio *et al* [47] reproduced the power-law distribution of the size of neuronal synchronization (known as neuronal avalanche) by a developing a network model. Modeling studies of recognition of ambiguous patterns have focused on fluctuations at the level of the neuron [48], [49]. For example, we revealed that chaotic neural activity leads to the emergence of the long-tailed distribution of residence time using an associative chaotic neural network model [48]. Furthermore, Kanamaru [49] revealed that the long-tailed distribution of residence time emerges in multiple coupled modules composed of spiking neural networks that exhibit chaotic activity. However, the factors that produce the characteristic long-tail remain controversial.

Furthermore, recent studies that focused on more physiological cortical structures, such as symmetricity of random synaptic connections and duality of complex synaptic connectivity, reported that these structures can reproduce complex spatiotemporal neural activity with slow temporal dynamics [33], [50], [51]. These slow temporal dynamics might contribute to the emergence of the long-tailed characteristic of temporal neural activity. As new candidates for these structures, it is known that cortical intermicrocircuit lateral connections in layers 2/3 of visual cortex [52]–[55] induce complex interactions of neural activity, including various temporal scale dynamics [56]–[58]. Moreover, such interlateral connections are not restricted to the visual cortex; they have been widely observed in the cerebral cortex for integrating information processing among different brain regions [59], [60]. To describe these complex mutual interactions of neural activity, a model-based numerical approach with spiking neural networks is considered appropriate, as it is difficult to apply an analytical approach in multibody systems with nonlinear dynamical interactions, even when the Fokker–Planck equations and mean-field approximations in the spiking neural networks [20], [61]–[63] were applied.

In this context, we hypothesized that spiking neural networks with interlateral and intralateral connections exhibiting a long-tailed EPSP distribution may induce complex neural activity with the long-tail characteristic of neural activity. We previously attempted to reproduce the spiking pattern alternation, given a long-tailed distribution of the switching period using coupled neural populations (called "neural modules" in this study) consisting of intramodule connections with log-normal EPSP distributions and excitatory intermodule connections inspired by cortical intermicrocircuit lateral connections [64]. However, no study to date has revealed the mechanisms underlying the spiking pattern alternation, provided a detailed evaluation of the complexity associated with temporal-scale dependence in dynamical spiking activity, or elucidated the conditions required to generate the long-tailed distribution of switching period patterns.

Therefore, in this study, we constructed spiking neural networks composed of two coupled modules with EPSPs following a log-normal distribution, based on the outcomes of our previous study [64]. First, we evaluated the spiking activity by power analysis and synchronization analysis in cases with and without large EPSPs. Second, we evaluated and compared the complexity of spiking dynamics and spiking pattern alternation between cases with and without large EPSPs. Third, we investigated the conditions required to generate the long-tailed distribution of switching period, in terms of the frequency of external stimulus and existence of intramodule connections with EPSPs following a log-normal distribution and intermodule connections.

II. MATERIAL AND METHODS

A. Spiking Neural Network

As shown in Fig. 1, we used two coupled spiking neural modules composed of excitatory and inhibitory neural populations. The excitatory-to-excitatory intramodule connections had synaptic weights following a log-normal distribution. Intermodule excitatory-to-excitatory and excitatory-to-inhibitory connections, which were inspired by interlateral connections in the cerebral cortex [52]–[55], joined two modules. We predicted that the spiking activity of each module suppressed the spiking activity of the other, given an adequately large magnitude of excitatory-to-inhibitory connections.

Terame *et al*. [20] proposed a spiking neural network that exhibits spontaneous activity using the log-normal distribution of EPSP. In this study, we employed this same spiking neural network. In each neuron of this network, the dynamics of the membrane potential $v(t)$ were given by the conductance, based on a leaky integrate-and-fire neuron model

$$\frac{dv}{dt} = -\frac{1}{\tau_m}(v - V_L) - g_E(v - V_E) - g_I(v - V_I) + I_{\text{ex}} \quad (1)$$

$$\text{if } v \geq V_{\text{thr}} \text{ [mV], then } v(t) \to V_r \quad (2)$$

where τ_m, V_E, V_I, and V_L are the membrane decay constants, and the reversal potentials of the α-amino-3-hydroxy-5-methyl-4-isoxazolepropionic acid-receptor-mediated excitatory synaptic current, inhibitory synaptic current, and leakage current, respectively. I_{ex} is an external input given by $21 \cdot \delta(t - t_{\text{ex}})$ [mV], where input time t_{ex} is drawn from a Poisson process with the input rate Λ [Hz], for the trigger to produce the spiking activity. The excitatory/inhibitory synaptic conductances $g_E(t)$ and $g_I(t)$ [ms^{-1}] were given by

$$\frac{dg_X}{dt} = -\frac{g_X}{\tau_s} + \sum_j G_{X,j} \sum_{s_j} \delta(t - s_j - d_j), \quad X = E, I \quad (3)$$

where τ_s is the decay constant of the excitatory and inhibitory synaptic conductances. s_j, d_j, $G_{E,j}$, and $G_{I,j}$ are spike times of synaptic input from the jth neuron, synaptic delays, and weights of excitatory and inhibitory synapses, respectively.

As the parameter sets of neurons, we used $V_I = -80$ [mV], $V_L = -70$ [mV], $V_r = -60$ [mV], $V_{\text{thr}} = -50$ [mV], $V_E = 0$ [mV], $\tau_m = 20$ [ms] (excitatory neuron), $\tau_m = 10$ [ms] (inhibitory neuron), and $\tau_s = 2$ [ms] [20]. In this study, (3) was solved using the Euler method, with the size of time step $\Delta t = 0.1$ [ms]. The refractory period was set to 1 [ms]. In this
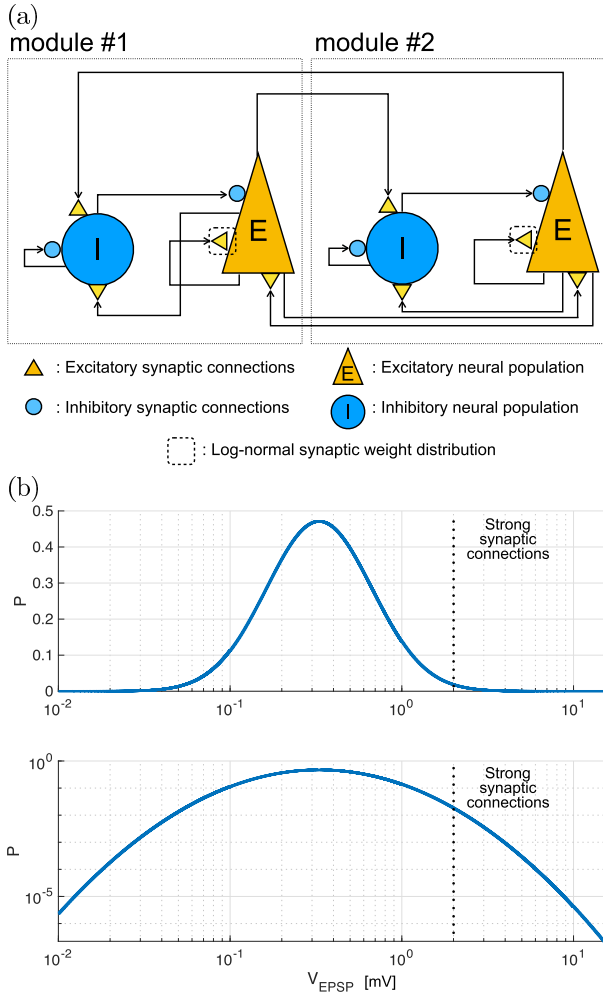
Fig. 1. (a) Topology of the spiking neural network. In the synaptic connections labeled by a dotted square, the EPSP follows a log-normal distribution. (b) Distribution of EPSP for intramodule excitatory-excitatory connections of the synaptic connections labeled by the dotted square in Fig. 1(a). Upper and lower parts show semilogarithmic and double-logarithmic charts, respectively.

study, the spiking neural network was simulated using Brian2 (https://brian2.readthedocs.io/en/2.0rc/index.html) [65].

For intramodule connections, the synaptic delays were set to uniform random values between 0 and 2 [ms]. The synaptic weights for excitatory-to-inhibitory, inhibitory-to-excitatory, and inhibitory-to-inhibitory connections were set to constant values of 0.018, 0.0019, and 0.0025, respectively. This parameter set was determined based on [20]. The size of the module was $N_E = 5000$ for excitatory neurons and $N_I = 1000$ for inhibitory neurons. For intramodule connections, each neuron was randomly connected with coupling probabilities, i.e., the probabilities of excitatory and inhibitory connections were 0.1 and 0.5, respectively.

For intermodule connections, each module was connected by excitatory-to-excitatory and excitatory-to-inhibitory synapses, whose strengths were $G_E = 0.05$ and 0.021. Each neuron was randomly connected with coupling probabilities, i.e., the probability of connections was 0.01. The synaptic delays were set to uniform random values between 1 and 3 [ms] and between 0 and 2 [ms] for the excitatory-to-excitatory and excitatory-to-inhibitory connections, respectively.

The amplitudes of EPSP, V_{EPSP} [mV], which represents increased membrane potential from the resting state, caused by excitatory synaptic input, were produced by a log-normal distribution, as follows [20]:

$$p(x) = \frac{\exp[-(\log x - \mu)^2/2\sigma^2]}{\sqrt{2\pi}\,\sigma x} \quad (4)$$

where $\sigma = 1.0$ and the mode of the distribution $\mu - \sigma^2 = \log 0.2$ was set. To remove unrealistic values of V_{EPSP} that exceeded 14 [mV], a new value was drawn from the distribution. We used this EPSP distribution for the intramodule excitatory-to-excitatory connections. To confirm the effect of the long-tail distribution, we compared the spiking activity between the case with strong synaptic weights ($V_{\text{EPSP}} > 2$ [mV]) and that without them. The synaptic transmissions failed with EPSP amplitude-dependence, according to the failing rate: $P_E = (a/a + V_{\text{EPSP}})$ ($a = 0.1$ [mV]) for excitatory-to-excitatory synaptic intermodule/intramodule connections [20], [26].

To translate V_{EPSP} as an observable value into synaptic weight G_E, we derived the relationship between V_{EPSP} and G_E as follows:

$$G_E = V_{\text{EPSP}}/100. \quad (5)$$

B. Evaluation Index

1) Spiking Rate: To observe temporal behaviors of spiking activity, we used spiking rates from the excitatory neural population of #j module r_E^j [Hz] and the inhibitory neural population r_I^j [Hz] as follows:

$$r_X^j(t) = 1000 \, \frac{S_X^j(t)}{\Delta t \, N_X} \quad X = E, I \quad (6)$$

where S_E^j/S_I^j indicates the frequency of spikes in the bin of width $\Delta t = 0.1$ [ms] in excitatory/inhibitory neural populations. Using these spiking rates, we measured the maintenance period of $r_E^1 > r_E^2$ or $r_E^2 > r_E^1$ as the residence time. Here, the time-series of spiking rate was smoothed by a moving average with a time window of 100 [ms]. The length of the time-series was set to 30 [s]. Using five types of seeds for randomization, we derived five time-series of spiking rates.

2) Power Spectrum Analysis: To analyze the temporal oscillation of spiking activity in the neural populations, power spectra for the time-series of spiking rates of $r_{E,I}^i$ were analyzed. The absolute power was calculated for these spectra. To estimate the power spectrum, we used a periodogram power spectral density.

3) Synchronization Index for Between Intermodule/Intramodule Neural Populations: In neural systems composed multiple neural populations, synchronization among temporal oscillation of spiking activity appears; this synchronization exhibits nonstationary temporal variability and frequency-band dependence [56]–[58]. To investigate this type of synchronization, an instantaneous phase approach utilizing the Hilbert transformation is widely utilized [66]–[69]. Therefore, to investigate synchronization of spiking activity in the intraneural/interneural modules,
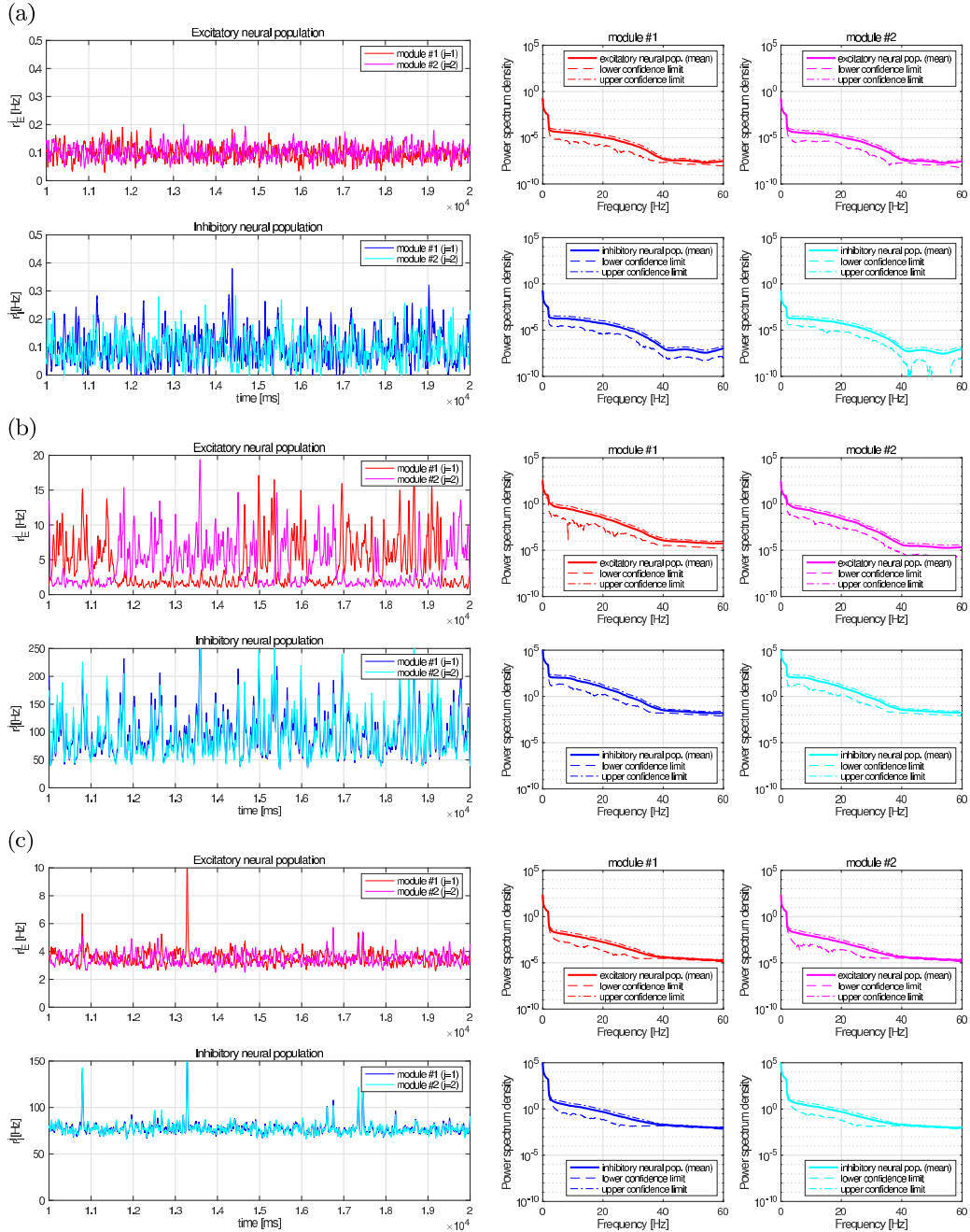
Fig. 2. Time-series of the spiking rate of excitatory and inhibitory neural populations (left) and their respective power spectrum (right) in the case with strong excitatory synaptic connections. (a) Poisson input spike rate $\Lambda = 0.1$ [Hz]. (b) $\Lambda = 0.3$ [Hz]. (c) $\Lambda = 2.0$ [Hz]. Here, mean values of power and the upper/lower confidence limits based on standard deviation were calculated from five time-series from different trials. In the $\Lambda = 0.3$ case, a state with high spiking rate $r_E^j \approx 10$ [Hz] (called the "activated state" in this study) appears intermittently and alternately between modules #1 and #2 (termed intermittent intermodule-alternative behavior). This behavior includes slow temporal behavior ([1:5] [Hz]).

we evaluated the phase synchronization (PS) of $r_{E,I}^i$ by using the PS index

$$\text{PS} = \cos(\Delta\theta) \qquad (7)$$

where $\Delta\theta$ indicates the phase difference between the spiking rates of $r_{E,I}^i$; each phase time-series of spiking rate is obtained by bandpass filtering with the range $[f_{\min} : f_{\max}]$ [Hz] and their Hilbert transformation. The $PS \approx 1.0, 0$, and -1.0 correspond to phase-coherent, nonphase-coherent, and antiphase-coherent

states, respectively. In this study, we focused on PS for the component $[f_{\min} : f_{\max}] = [10 : 20]$ [Hz].

4) Multiscale Entropy: The temporal fluctuation of neural activity, which is observed in experimental observations of neural activity, such as EEG/MEG, and in the reproduced temporal oscillation of spiking activity by spiking neural networks, has been shown to exhibit nonstationary temporal variability and frequency-band dependence [1]–[6], [33], [64]. To characterize the complexity of the temporal neural activity, multiscale entropy (MSE) [70] has been widely
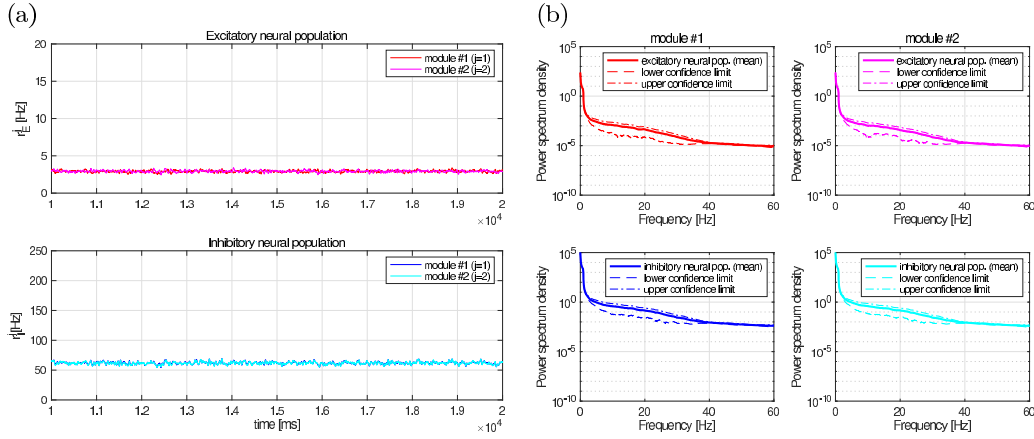
Fig. 3. (a) Time-series of the spiking rate of excitatory and inhibitory neural populations in the case without strong excitatory synaptic connections. Λ is set to 3.0 [Hz] to obtain the mean excitatory spiking rate of r_E^j corresponding to that of r_E^j in Fig. 2(b), i.e., ≈ 3.0 [Hz] ($\Lambda = 0.3$ [Hz] case). (b) Power spectrum for the spiking rate $r_{E,I}^j$. Here, mean values of power and upper/lower confidence limits based on standard deviation were calculated from five time-series from different trials. The intermittent intermodule-alternative behavior observed in the case with strong synaptic connections (see Fig. 2) does not occur.

utilized [1], [33], [64]. Therefore, to evaluate the temporal-scale dependence of the complexity in the time series of r_E^j, MSE was employed in this study. MSE is the sample entropy (SampEn) at each temporal scale factor τ ($\tau = 1, 2, \ldots$). The SampEn for stochastic variables $\{x_1, x_2, \ldots, x_N\}$ is defined by

$$h^\tau(r, m) = -\log \frac{C_{m+1}(r)}{C_m(r)} \quad (8)$$

where $C_m(r)$ indicates the probability of satisfying $|\mathbf{x}_i^m - \mathbf{x}_j^m| < r$ ($i \neq j$, $i, j = 1, 2, \ldots$). $\mathbf{x}_i^m$ is an m-dimensional vector $\mathbf{x}_i^m = \{x_i, x_{i+1}, \ldots, x_{i+m-1}\}$.

In the MSE analysis, the sample entropy $h^\tau(r, m)$ was calculated against the temporal coarse-grained series $\{x_1, x_2, \ldots, x_N\}$, with the scale factor τ

$$y_j^{(\tau)} = \frac{1}{\tau} \sum_{i=(j-1)\tau+1}^{j_\tau} x_i. \quad (1 \leq j \leq N/\tau). \quad (9)$$

Using the dependence of $h^\tau(r, m)$ on the scale factor τ, the characteristic of the complexity in the time-series of the excitatory firing rates r_E^j was evaluated. In this study, we set $m = 2$, $r = 0.2$ [70], and the scale width to 10 [ms].

5) Surrogate Data Analysis: Recent findings regarding temporal fluctuations of neural activity imply that the structural network characteristics induce complex temporal neural fluctuation [20], [29]–[33]. Moreover, we previously reported that this characteristic appears as the deterministic dynamical activity, instead of stochastic temporal behavior [33]. To investigate whether the complexity of temporal spiking activity is produced by a deterministic or stochastic process, we utilized the surrogate data analysis. We derived the surrogate data by using iterative amplitude adjusted Fourier transform (IAAFT) surrogate data analysis for the spiking rate r_E^j to examine whether a nonlinear dynamic process is involved in the spiking rates [71]. To retain the power spectrum density profile of the original time-series, 30 iterations were performed [71]. We compared the MSE profile between the original time-series r_E^j and that for IAAFT. Here, using five types of seeds for randomization, we derived five surrogate data sets per time-series r_E^j and then calculated an average value among the corresponding SampEn values. To evaluate the differences between MSE profiles of the original time-series of r_E^j and that for IAAFT, a paired t-test was used. A two-tailed α level of 0.01 and 0.001 was considered statistically significant.

III. RESULTS

A. Neural Activity in Networks With/Without Strong Excitatory Synaptic Connections

Fig. 2 (left) shows the time-series of spiking rate $r_{E,I}^j$, given strong excitatory synaptic connections when applying the Poisson input spikes with $\Lambda = 0.1, 0.3, 2.0$ [Hz]. In the $\Lambda = 0.3$ [Hz] case, the spiking rates exhibited greater temporal variability than the counterparts when applying the Poisson input spikes with smaller and larger values of Λ ($\Lambda = 0.1, 2.0$). In particular, the state with high spiking rate $r_E^j \approx 10$ [Hz] (called an "activated state" in this study) appeared intermittently and alternately between modules #1 and #2 (termed "intermittent intermodule-alternative behavior"). Conversely, in the case without strong synaptic connections, the large variability and alternation of spiking rate were not confirmed (see Fig. 3). These power spectrum densities primarily distributed from [0:30] [Hz] in both network cases, as shown in the right-hand side of Figs. 2 and 3. In particular, in the case with strong excitatory synaptic connections and $\Lambda = 0.3$ [Hz], the slow frequency component of power ([1:5] [Hz]), which corresponds to the intermittently alternative behavior observed in Fig. 2(b), increased in comparison with the other cases.

B. Phase Synchronization Analysis

The intermittent intermodule-alternative behavior was analyzed with respect to PS. Fig. 4 shows the time-series of differences in spiking rates for $r_E^1 - r_E^2$ and $r_I^1 - r_I^2$ and the time-series of phase-synchronization (PS) indexes betweenintermodule excitatory-excitatory/inhibitory-inhibitory neural populations (r_E^1/r_E^2 and r_I^1/r_I^2) and for intramodule
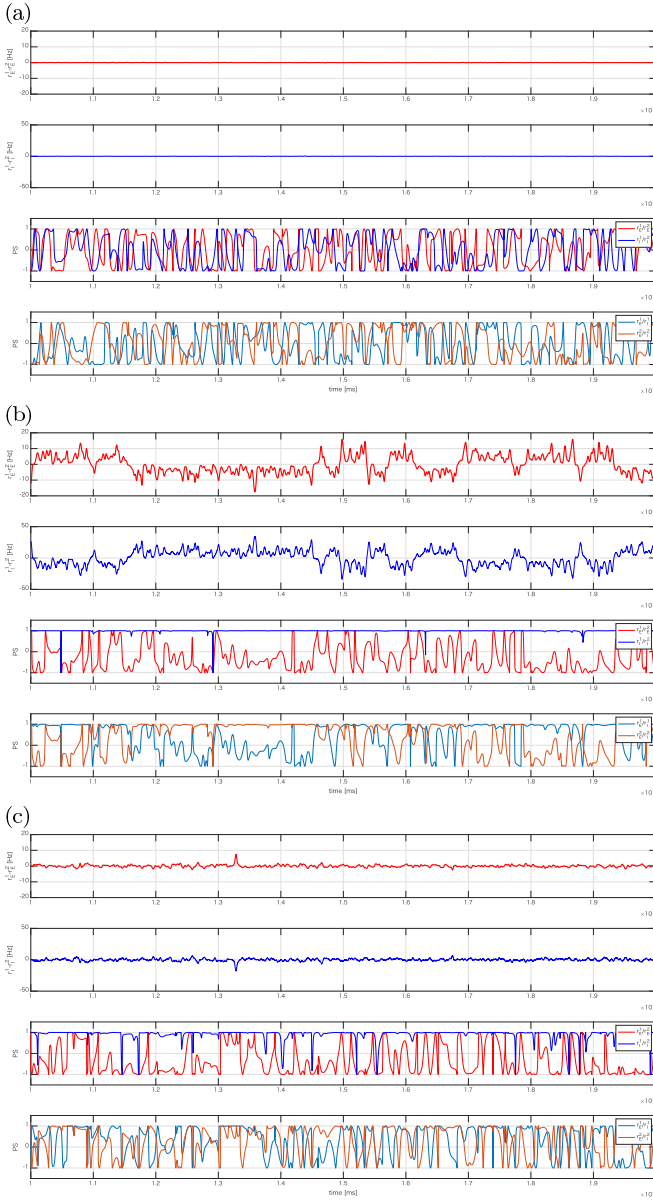
Fig. 4. Time-series of the difference in spiking rates of $r_E^1 - r_E^2$ [Hz] and $r_I^1 - r_I^2$ [Hz] (top two figures) in the case with strong EPSP connections. Time-series of PS indexes between interneural modules (r_E^1/r_E^2 and r_I^1/r_I^2) and intraneural modules (r_E^1/r_I^1 and r_E^2/r_I^2) (bottom two figures). (a) $\Lambda = 0.1$ [Hz]. (b) $\Lambda = 0.3$ [Hz]. (c) $\Lambda = 2.0$ [Hz]. These results were calculated using the spiking rate shown in Fig. 2. In the $\Lambda = 0.3$ [Hz] case, the time-series $r_E^1 - r_E^2$ and $r_I^1 - r_I^2$ act in opposition. Regarding PS, the phases of the intramodule-excitatory–inhibitory neural population, corresponding to the module with $r_E^1 > r_E^2$ or $r_E^2 > r_E^1$, synchronized (PS $\approx$ 1.0). Strong PS between intermodule-inhibitory-inhibitory neural populations was confirmed (PS $\approx$ 1.0).

excitatory–inhibitory neural populations (r_E^1/r_I^1 and r_E^2/r_I^2) in $\Lambda = 0.1, 0.3, 2.0$ [Hz] cases. For the weak input frequency $\Lambda = 0.1$ [Hz] case, intermodule-alternative behavior was not confirmed ($r_E^1 - r_E^2 \approx 0$ [Hz] and $r_I^1 - r_I^2 \approx 0$ [Hz]). The time-series of the PS index almost always changed the values in $-1.0 \leq PS \leq 1.0$ in inter/intra modules, i.e., PS did not arise. In the moderate input frequency case $\Lambda = 0.3$ [Hz], there was intermittent alternation of positive and negative values of $r_E^1 - r_E^2$ and $r_I^1 - r_I^2$. Here, the time-series of $r_E^1 - r_E^2$ and $r_I^1 - r_I^2$ behaved in
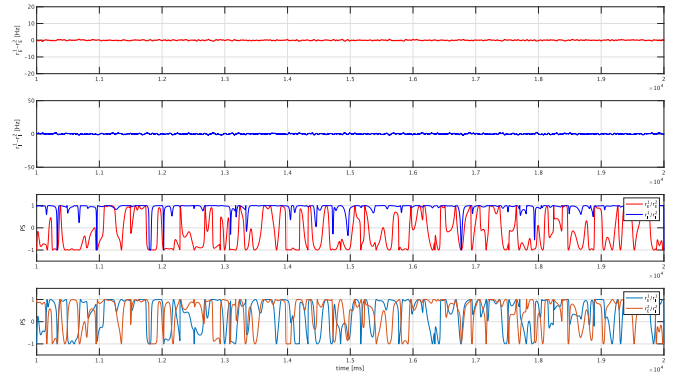

Fig. 5. Time-series of the difference in spiking rates of $r_E^1 - r_E^2$ [Hz] and $r_I^1 - r_I^2$ [Hz] (top two figures) in the case without strong EPSP connections. Time-series of the PS indexes between interneural modules (r_E^1/r_E^2 and r_I^1/r_I^2) and intraneural modules (r_E^1/r_I^1 and r_E^2/r_I^2) (bottom two figures). These results were calculated using the spiking rate shown in Fig. 3. The explicitly intermittent alternations of $r_E^{1,2}$ and $r_I^{1,2}$ were not confirmed, and the period of synchronization of intramodule-excitatory–inhibitory neural populations (r_E^1/r_I^1 and r_E^2/r_I^2) was shorter in comparison with that in the $\Lambda = 0.3$ [Hz] case with strong EPSP connection [see Fig. 4(b)].

opposition. That is, activation of the module was induced by deactivation of the inhibitory neural population within the module. Regarding PS, we confirmed the tendency of phases of the intramodule-excitatory–inhibitory neural populations, corresponding to the module with $r_E^1 > r_E^2$ or $r_E^2 > r_E^1$, to synchronize (PS $\approx$ 1.0). For the phases of the intermodule-excitatory-excitatory/intermodule-inhibitory-inhibitory neural populations, strong PS of intermodule-inhibitory-inhibitory neural populations was confirmed (PS $\approx$ 1.0). In the high input frequency $\Lambda = 2.0$ [Hz] case, the explicitly intermittent alternations of $r_E^{1,2}$ and $r_I^{1,2}$ were not confirmed, and the period of synchronization of intramodule-excitatory–inhibitory neural populations (r_E^1/r_I^1 and r_E^2/r_I^2), which were observed in the $\Lambda = 0.3$ [Hz] case, became shorter. In addition to the case with strong EPSP connections, the result of the case without strong EPSP connections is shown in Fig. 5. The explicitly intermittent alternations of $r_E^{1,2}$ and $r_I^{1,2}$ were not confirmed, and the period of intramodule-excitatory–inhibitory synchronization (r_E^1/r_I^1) and (r_E^2/r_I^2) was shorter in comparison with that of the $\Lambda = 0.3$ [Hz] case with strong EPSP connections [see Fig. 4(b)].

To elucidate the relationship between absolute power and PS, the normalized duration of PS (duration rate accounting for PS > 0.9) and absolute power were investigated. Fig. 6(a) shows the scatter plots of the temporal average of the spiking rate r_E^j [Hz] and the absolute power in the range [10:20] [Hz]. Here, these values were averaged among modules #1 and #2. The input frequency Λ was set to 0.1, 0.2, 0.3, 0.4, 0.5, 0.6, 0.7, 0.8, 0.9, 1.0, and 2.0 [Hz] in the case with strong EPSP connections and 1.0, 2.0, 3.0, 4.0, and 5.0 [Hz] in the case without strong EPSP connections. Fig. 6(b) shows the scatter plots of the temporal average of spiking rate r_E^j [Hz] and the normalized duration of $PS > 0.9$ for intramodule-excitatory–inhibitory synchronization under the same conditions as that in Fig. 6(a). The results indicated that the power and intramodule-excitatory–inhibitory synchronizations enhanced with increasing excitatory spiking activity
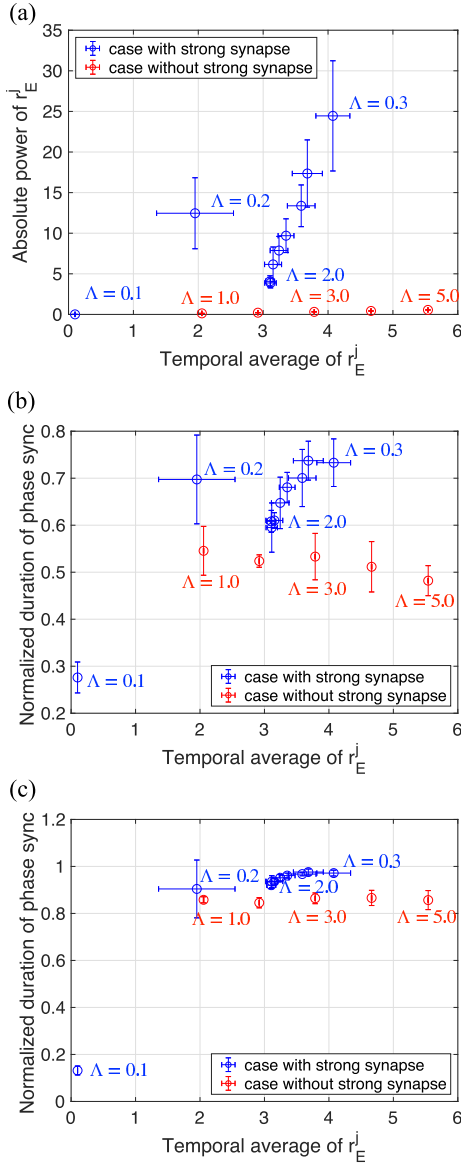
(a)

(b)

(c)

Fig. 6. (a) Scatter plots of the temporal average of r_E^j and absolute power in the range [10:20] [Hz]. Here, these values were averaged among modules. (b) Scatter plots of the temporal average of r_E^j and normalized duration of PS > 0.9 in intraneural modules (r_E^1/r_I^1 and r_E^2/r_I^2). (c) Scatter plots of the temporal average of r_E^j and normalized duration of PS > 0.9 in interinhibitory neural populations (r_I^1/r_I^2). The input frequency Λ is set to 0.1, 0.2, 0.3, 0.4, 0.5, 0.6, 0.7, 0.8, 0.9, 1.0, and 2.0 [Hz] in the case with strong EPSPs and 1.0, 2.0, 3.0, 4.0, and 5.0 [Hz] in the case without strong EPSPs; typical Λ values were represented by blue text (case with strong EPSPs) and red text (case without strong EPSPs). Solid circles indicate mean values corresponding to the horizontal/vertical labels among five trials. Horizontal and vertical error bars show their standard deviation. In the case with strong EPSPs, the absolute power and phase synchronized duration increased as the temporal average of r_E^j increased in comparison with the cases without strong EPSPs.

in the case with strong EPSP connections; they became higher at the appropriate input frequency $\Lambda \approx 0.3$ [Hz] in comparison with the other Λ cases, i.e., the oscillation power for spiking rate and intramodule-excitatory–inhibitory synchronization were strongly correlated with each other. In Fig. 6(c), scatter plots of the temporal average of the spiking rate r_E^j and the normalized duration of $PS > 0.9$ for intermodule-inhibitory-inhibitory synchronization were shown. Here, the condition is

the same as that in Fig. 6(a) and (b). The results showed that the case with strong EPSP connections accomplished a longer duration of intermodule-inhibitory-inhibitory synchronization at the same temporal average of excitatory spiking rate.

C. Multiscale Entropy Analysis

Fig. 7 shows the MSE profile against the time-series of r_E^j for the case with strong synaptic connections (corresponding to r_E^j in Fig. 2). In $\Lambda = 0.1, 2.0$ [Hz] cases, the MSE profiles exhibited a unimodal maximum peak at approximately $\tau \approx 10$ (100 [Hz]). However, in the $\Lambda = 0.3$ [Hz] case, the peak decreased and the values of h^τ increased at a larger temporal scale [$\tau \gtrsim 200$ (5 [Hz])].

Moreover, we compared the values of h^τ in the original spiking rate r_E^j with those in the IAAFT surrogate data. The h^τ values in the case of $\Lambda = 0.3$ [Hz] were significantly lower at $\tau \approx 100$ (10 [Hz]) than in the surrogate data produced using IAAFT. Therefore, it can be interpreted that this MSE profile in the $\Lambda = 0.3$ [Hz] case reflects a deterministic process of the spiking neural network. Regarding the case without excitatory strong synaptic connections, Fig. 8 shows its MSE profile against the time-series of r_E^j, corresponding to Fig. 3. The same MSE profile occurred as in $\Lambda = 0.1, 2.0$ [Hz] cases with strong synaptic connections, i.e., a unimodal maximum peak at approximately $\tau \approx 10$ (100 [Hz]); temporal scales τ satisfying significant differences of h^τ versus the IAAFT surrogate data were few.

D. Characteristics of Alternation of Activate and Deactivate States

Against these time-series of r_E^j in both cases with and without strong synaptic connections, the residence time distribution was represented, as shown in Fig. 9. In cases with ($\Lambda = 0.1, 2.0$ [Hz]) and without strong synaptic connections, the peak value was approximately 20 [ms]. However, in the case with strong synaptic connections ($\Lambda = 0.3$ [Hz]), the peak shifted to 220 [ms], and the probability density at $\gtrsim 220$ [ms] increased, i.e., a long-tailed distribution appeared.

IV. CONCLUSION AND DISCUSSION

In this study, we constructed two coupled modules of spiking neural networks with excitatory and inhibitory neural populations possessing a log-normal EPSP distribution. We evaluated spiking activities given different input frequencies of the Poisson process in the cases with/without strong EPSP connections. Coupled modules exhibited intermittent intermodule-alternative behavior, given moderate input frequency and the existence of strong EPSP connections. In this behavior, the phases of the intramodule-excitatory–inhibitory neural population in the activated state and that of the intermodule-inhibitory-inhibitory neural population synchronized. Using the MSE analysis, we revealed that this intermodule-alternative behavior enhanced the complexity of spiking activity at larger temporal scales. Furthermore, the surrogate analysis of spiking activity in cases with/without strong EPSP connections revealed that the complexity at large
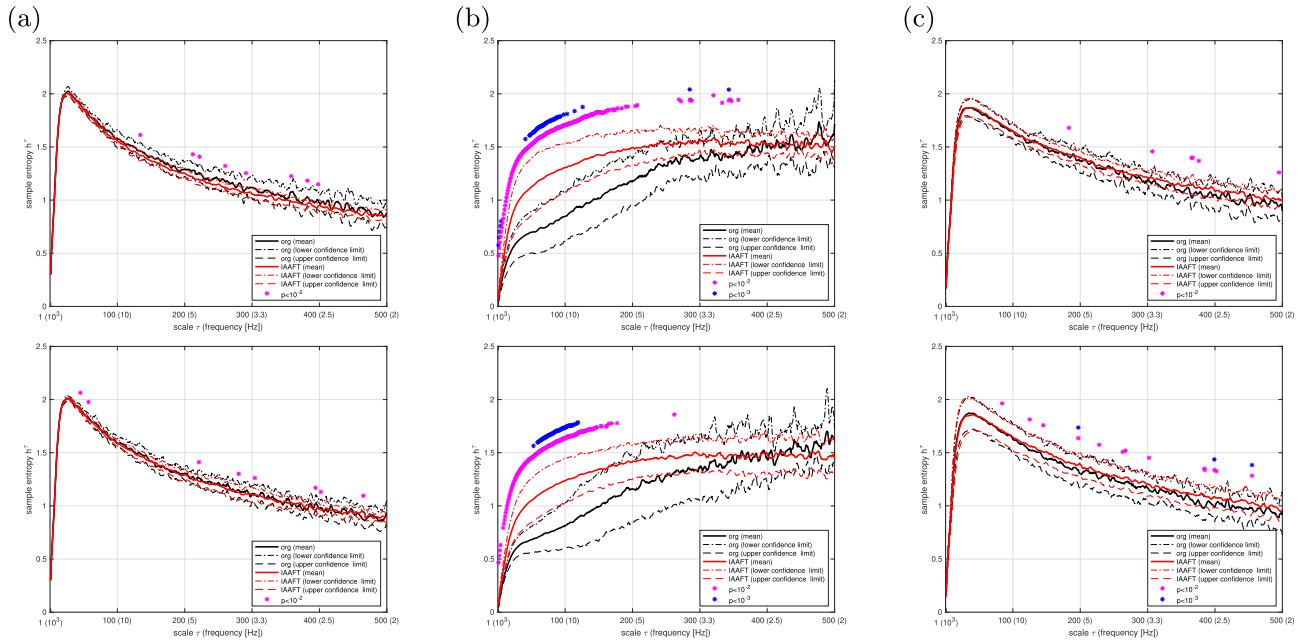
Fig. 7. Dependence of sample entropy h^τ on scale factor τ in r_E^j in cases with strong excitatory synaptic connections. This condition is same in Fig. 2. Upper and lower figures represent modules #1 ($j = 1$) and #2 ($j = 2$). (a) $\Lambda = 0.1$ [Hz]. (b) $\Lambda = 0.3$ [Hz]. (c) $\Lambda = 2.0$ [Hz]. Here, the mean values of h^τ and upper/lower confidence limits based on standard deviation were calculated from five time-series from different trials. Magenta and blue $*$ indicate cases satisfying $p < 0.01, 0.001$, respectively, for paired t-tests between the values of h^τ of the original r_E^j and those of the surrogate data produced using IAAFT. In the $\Lambda = 0.3$ [Hz] case, the values of h^τ increased at a larger temporal scale [$\tau \gtrsim 200$ (5 [Hz])]. These values were significantly lower at $\tau \approx 100$ (10 [Hz]) in comparison with the surrogate data produced using IAAFT.

temporal scales was induced by nonlinear neural dynamics. Furthermore, by comparing the residence time between cases with and without strong EPSP connections, we revealed that these strong EPSP connections played a crucial role in the emergence of the heavy-tailed distribution of this characteristic.

First, we must consider the reason that the activated state was induced by a moderate input frequency $\Lambda = 0.3$ [Hz] in the network with strong EPSP connections. When the spiking rate of one module increased, the excitatory and inhibitory spiking activity of this module synchronized, particularly in the network with strong EPSP connections [see Fig. 6(b)]. It is known that local interactions between excitatory and inhibitory neurons induce neural oscillations with high coherence between excitatory and inhibitory neural populations [72]–[76], and the size of this synchronized neural population is expanded under strong EPSP connections [29]. Therefore, it can be interpreted that the activated state of one module corresponded to the oscillation induced by intramodule connections between excitatory and inhibitory neural populations and the existence of strong EPSP connections, whereas the deactivated state of the other module represented subserviently spiking activity driven by the external input spikes and spikes from other modules.

Moreover, this oscillation in the excitatory neural population leads to high phase coherence of interinhibitory-inhibitory neural populations because both inhibitory neural populations were always applied via spikes from either module #1's or #2's activated excitatory neural population [see Fig. 6(c)]. Here, although the activated state of the excitatory neural population alternated to the other excitatory neural population, the spikes

of the alternating excitatory neural population affected both inhibitory neural populations. These spikes were the common input for both inhibitory neural populations; therefore, strong synchronization of intermodule-inhibitory-inhibitory neural populations occurred. Many studies have reported that the synchronization of the inhibitory neural populations supports cognitive functions involving memory formation and sensory processing [77], [78] (reviewed in [76]). The synchronization between interinhibitory-inhibitory neural populations observed in this study might explain the mechanism for the inhibitory synchronization. For weak input frequencies, such as the $\Lambda = 0.1$ [Hz] case in Fig. 4, the excitatory spiking activity (r_E^i) was too low to induce oscillation and synchronization; in contrast, disturbance by a large input frequency, such as the $\Lambda = 2.0$ [Hz] case in Fig. 4, degrades them.

Furthermore, it is necessary to consider why the activated state alternated between the modules in the intermittent intermodule-alternative behavior. Previous studies have reported that the log-normal synaptic weight distribution exhibits large variability in neural activity [9]. Therefore, highly variable spiking activity can unlock the synchronization between intramodule excitatory and inhibitory neural populations. The unlocked state decreases neural oscillations in the module. This leads to decreased inhibitory spiking activity in the other module due to decreased excitatory synaptic inputs; subsequently, the activated state of the other modules arises. Previous model-based studies that used log-normal EPSP connections reported that multiple states of neural activity were constructed, and alternative switching arises [31]. Furthermore, in a study of interlateral connections without log-normal synaptic weight distribution, alternative switching
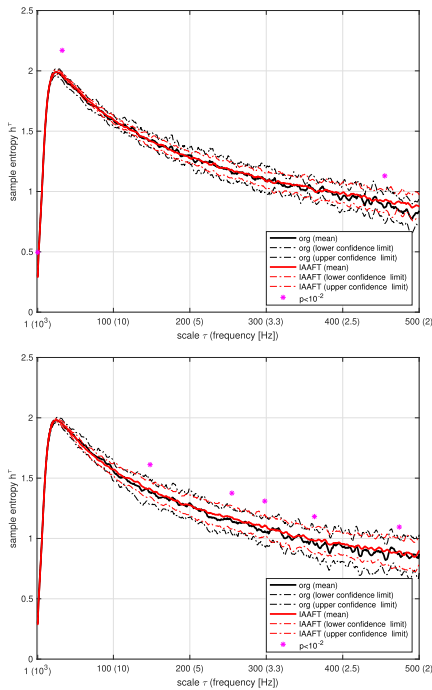
Fig. 8. Dependence of sample entropy h^τ on scale factor τ in r_E^j in the case without strong excitatory synaptic connections. The condition is the same as that in Fig. 3. Upper and lower figures represent modules #1 ($j = 1$) and #2 ($j = 2$). Here, the mean values of h^τ and upper/lower confidence limits based on standard deviation were calculated from five time-series from different trials. Magenta $*$ indicates the cases satisfying $p < 0.01$ for paired t-tests between the values of h^τ of the original r_E^j and those of the surrogate data produced using IAAFT. A unimodal maximum peak was present at approximately $\tau \approx 10$ (100 [Hz]), and temporal scales τ satisfying significant differences of h^τ versus the IAAFT surrogate data were few. This tendency was also present for cases with $\Lambda = 0.1, 2.0$ [Hz] and strong synaptic connections [see Fig. 7(a) and (c)].

was not reported [56]. Moreover, the results of our PS analysis in the case without strong EPSP connections showed the same tendency (see Fig. 5). Therefore, the log-normal synaptic weight distribution has a crucial role in inducing this alternation. For larger input frequencies (such as $\Lambda = 2.0$ [Hz] case in Figs. 2 and 4) case with strong EPSP connections, it can be interpreted that the external high-frequency input becomes dominant in comparison with the excitatory–inhibitory interaction. Therefore, the explicit alternation with a large period is broken.

The relationship of the MSE profile and the residence time distribution with the intermittent intermodule-alternative behavior must be considered. The probability density of residence time at $\Lambda = 0.3$ [Hz] becomes higher than the other input frequency in the case without strong synapses in the region $\gtrsim 200$ [ms]; SampEn in the temporal scale region [$\tau > 20$ (corresponding frequency/period: 5 [Hz]/200 [ms])] becomes higher. This temporal scale region is congruent with the temporal scale required for the alternatively switching activated state behavior, as indicated by the power spectrum analysis. Moreover, the results of the IAAFT surrogate data analysis indicate that the MSE profile in $\tau > 20$ at $\Lambda = 0.3$ [Hz] reflects a nonlinear deterministic process of the spiking neural network. This behavior was not confirmed in

the single isolated module case (see Appendix A) or the case without strong synaptic connections. Therefore, these alternation behaviors with slow temporal scale dynamics were induced by intermodule synaptic connections and intramodule long-tailed synaptic connections.

The application of the results of this study must be considered. Recently, by the virtue of proposing several methods of backpropagation for spiking neural networks, the application of spiking neural networks to machine learning has been rapidly progressing [79]–[87]. However, these types of spiking neural networks do not exhibit complex dynamic behavior because most do not possess recurrent structures and use too simple a spiking neuron model. Nevertheless, Bellec *et al.* [88] showed that neural dynamics and recurrent structure might enhance the learning ability of a network. In addition, Hiratani *et al.* [89] demonstrated that the irregular complex spiking behavior produced by the log-normal synaptic weight distribution may enhance memory recall in a recurrent spiking neural network. Therefore, the long-tailed distribution of synaptic weight, which can produce complex temporal-scale-dependent dynamics, might be utilized to enhance the ability of machine learning using spiking neural networks. To achieve this purpose, further evaluation of the functionality of neural activity using the log-normal characteristics is needed.

The limitations of this study must be considered. This study dealt with intermodule-alternative behavior using a numerical model-based approach within a spiking neural network. However, to achieve a general description of this characteristic, an analytical approach is needed. Although an analytical approach to a multibody system with nonlinear dynamics is difficult, the recent progress reported in the studies of the Fokker–Planck equations in spiking neural networks [90], [91] might provide an effective solution for this purpose. In addition, the neural activity in this study was induced by random input spikes from the Poisson process. However, a recent study reported that the oscillation of neural activity in the theta to beta bands frequency range (8–30 Hz) plays a role in signal transmission among interneural module connections [58]. Therefore, neural activity driven by these neural oscillations in coupled modules should be evaluated. Furthermore, the evaluation of neural activity where EPSPs follow other long-tailed EPSP distribution is needed. As a part of a preliminary evaluation, we have confirmed intermittent intermodule-alternative behavior with large temporal scale behavior, similar to that observed for log-normal distribution (see Appendix. B).

We conclude that long-tailed synaptic weight distribution and intermodule synaptic connections enhance the complexity of spiking activity at large temporal scales and induce nonlinear dynamics and neural activity following a long-tailed distribution.

APPENDIX A
NEURAL ACTIVITY IN AN ISOLATED MODULE

Fig. 10 shows the time-series of spiking rates r_E and r_I in a single-module case ($\Lambda = 0.3$ [Hz]) where the intramodule
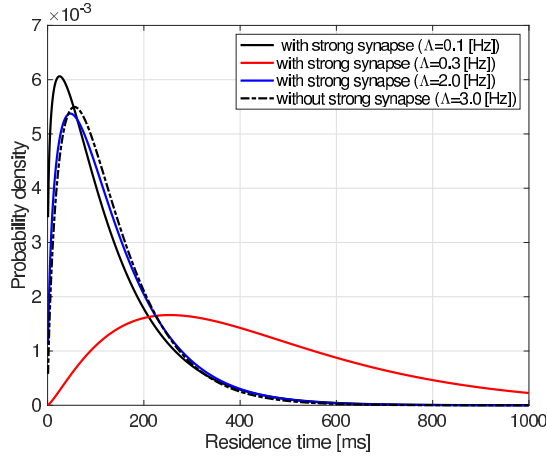
Fig. 9. Residence time distribution for cases with and without strong synapses. Here, the probability density was estimated using a gamma distribution. In the case with strong synaptic connections ($\Lambda = 0.3$ [Hz]), the peak shifted to 220 [ms], and the probability density at $\gtrsim 220$ [ms] increased, i.e., a long-tailed distribution appeared.
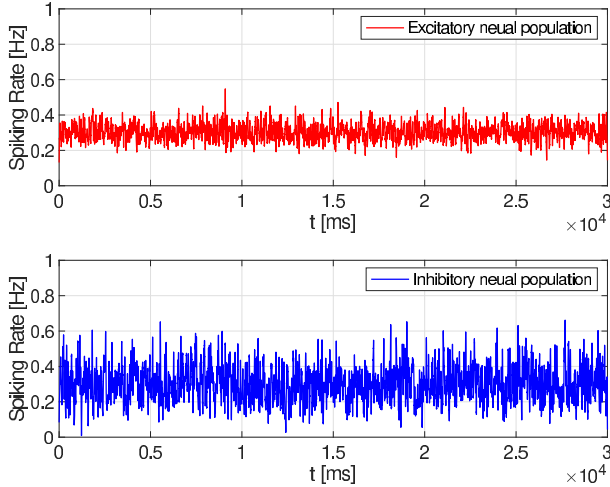

Fig. 10. Time-series of spiking rate r_E and r_I in a single-module case ($\Lambda = 0.3$ [Hz]). In this condition, the intermittent intermodule-alternative behavior, which was observed in the two coupled modules, did not arise.

parameters were set to ensure a long-tailed distribution of residence time (corresponding to the $\Lambda = 0.3$ [Hz] case in Fig. 9). In this condition, spiking rates remained approximately at the applied external input frequency $\Lambda = 0.3$ [Hz], and the intermittent intermodule-alternative behavior, which was observed in the case of two coupled modules, did not arise.

APPENDIX B
NEURAL ACTIVITY IN A CASE WITH ANOTHER LONG-TAILED EPSP DISTRIBUTION

In addition to log-normal distribution, the gamma distribution is a typical long-tailed distribution. We evaluated the neural activity in the spiking neural network with EPSP amplitudes following gamma distribution given by

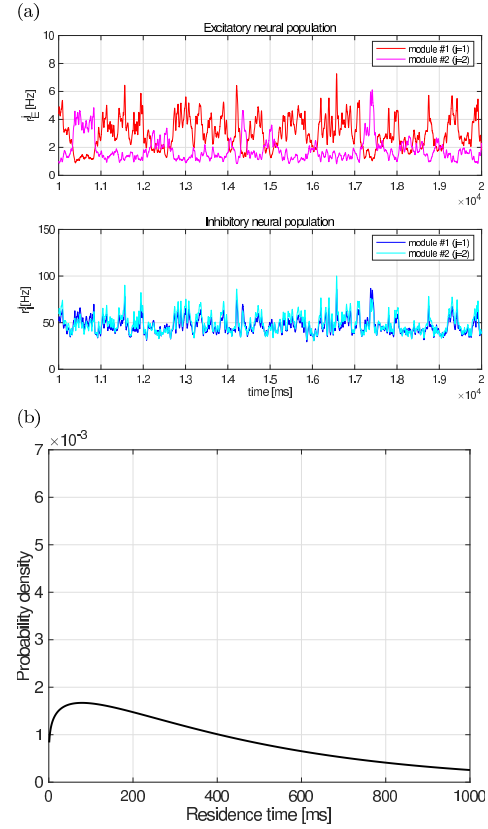$$p(x) = \frac{x^{\alpha-1} e^{-x/\beta}}{\beta^\alpha \Gamma(\alpha)} \tag{10}$$

Fig. 11. (a) Time-series of the spiking rate of excitatory and inhibitory neural populations in the case for EPSP following a gamma distribution. (b) Its respective residence time distribution. Here, the probability density was estimated using a gamma distribution. The probability density at $\gtrsim 220$ [ms] increased more in comparison with the case without strong EPSP connection in Fig. 9, i.e., a long-tailed distribution appeared.

where $\Gamma(\cdot)$ is a gamma function and α and β were shape and scale parameters. These parameters were set as $\beta = 0.76, \alpha = 0.2/\beta + 1 \approx 1.263$ to obtain the same mode of $p(x)$ in the log-normal distribution $V_{\text{EPSP}} = 0.2$ [mV] and, approximately, the same number of synaptic weights $V_{\text{EPSP}} > 2$ [mV]. The other conditions were the same as those in the spiking neural network with log-normal EPSP.

Fig. 11(a) shows the time-series of spiking rate $r_{E,I}^j$ when applying the Poisson input spikes with $\Lambda = 0.4$ [Hz]. The results show that the intermittent intermodule-alternative behavior is similar to that where EPSP follows a log-normal distribution. The residence time distribution is shown in Fig. 11(b); the probability density at $\gtrsim 200$ [ms] is higher in comparison with the case without strong EPSP connection in Fig. 9, i.e., a long-tailed distribution appeared.

REFERENCES

[1] T. Takahashi et al., "Quantitative evaluation of age-related white matter microstructural changes on MRI by multifractal analysis," J. Neurological Sci., vol. 225, nos. 1–2, pp. 33–37, Oct. 2004.
[2] A. R. McIntosh, N. Kovacevic, and R. J. Itier, "Increased brain signal variability accompanies lower behavioral variability in development," PLoS Comput. Biol., vol. 4, no. 7, Jul. 2008, Art. no. e1000106.
[3] D. D. Garrett, N. Kovacevic, A. R. McIntosh, and C. L. Grady, "Blood oxygen level-dependent signal variability is more than just noise," J. Neurosci., vol. 30, no. 14, pp. 4914–4921, Apr. 2010.
[4] D. D. Garrett, N. Kovacevic, A. R. McIntosh, and C. L. Grady, "The importance of being variable," J. Neurosci., vol. 31, no. 12, pp. 4496–4503, 2011.

[5] T. Takahashi, "Complexity of spontaneous brain activity in mental disorders," *Prog. Neuro-Psychopharmacol. Biol. Psychiatry*, vol. 45, pp. 258–266, Aug. 2013.

[6] A. C. Yang and S.-J. Tsai, "Is mental illness complex? From behavior to brain," *Prog. Neuro-Psychopharmacol. Biol. Psychiatry*, vol. 45, pp. 253–257, Aug. 2013.

[7] E. Bullmore and O. Sporns, "Complex brain networks: Graph theoretical analysis of structural and functional systems," *Nature Rev. Neurosci.*, vol. 10, no. 3, pp. 186–198, Mar. 2009.

[8] O. Sporns, "Contributions and challenges for network models in cognitive neuroscience," *Nature Neurosci.*, vol. 17, no. 5, pp. 652–660, May 2014.

[9] G. Buzsáki and K. Mizuseki, "The log-dynamic brain: How skewed distributions affect network operations," *Nature Rev. Neurosci.*, vol. 15, no. 4, pp. 264–278, Apr. 2014.

[10] D. S. Bassett and O. Sporns, "Network neuroscience," *Nature Neurosci.*, vol. 20, no. 3, pp. 353–364, 2017.

[11] J. Fell, A. Kaplan, B. Darkhovsky, and J. Röschke, "EEG analysis with nonlinear deterministic and stochastic methods: A combined strategy," *Acta Neurobiologiae Experimentalis*, vol. 60, no. 1, pp. 87–108, 1999.

[12] V. M. Eguíluz, D. R. Chialvo, G. A. Cecchi, M. Baliki, and A. V. Apkarian, "Scale-free brain functional networks," *Phys. Rev. Lett.*, vol. 94, no. 1, Jan. 2005, Art. no. 018102.

[13] P. Hagmann *et al.*, "Mapping human whole-brain structural networks with diffusion MRI," *PLoS ONE*, vol. 2, no. 7, p. e597, Jul. 2007.

[14] P. Hagmann *et al.*, "Mapping the structural core of human cerebral cortex," *PLoS Biol.*, vol. 6, no. 7, p. e159, Jul. 2008.

[15] M. van den Heuvel, R. Mandl, J. Luigjes, and H. H. Pol, "Microstructural organization of the cingulum tract and the level of default mode functional connectivity," *J. Neurosci.*, vol. 28, no. 43, pp. 10844–10851, 2008.

[16] M. P. van den Heuvel and O. Sporns, "Network hubs in the human brain," *Trends Cognit. Sci.*, vol. 17, no. 12, pp. 683–696, Dec. 2013.

[17] Q. She, G. Chen, and R. H. M. Chan, "Evaluating the small-worldness of a sampled network: Functional connectivity of entorhinal-hippocampal circuitry," *Sci. Rep.*, vol. 6, no. 1, p. 21468, Aug. 2016.

[18] T. P. Vogels and L. F. Abbott, "Signal propagation and logic gating in networks of integrate-and-fire neurons," *J. Neurosci.*, vol. 25, no. 46, pp. 10786–10795, 2005.

[19] D. Guo and C. Li, "Self-sustained irregular activity in 2-D small-world networks of excitatory and inhibitory neurons," *IEEE Trans. Neural Netw.*, vol. 21, no. 6, pp. 895–905, Jun. 2010.

[20] J.-N. Teramae, Y. Tsubo, and T. Fukai, "Optimal spike-based communication in excitable networks with strong-sparse and weak-dense links," *Sci. Rep.*, vol. 2, no. 1, pp. 1–6, Dec. 2012.

[21] N. M. Timme *et al.*, "High-degree neurons feed cortical computations," *PLOS Comput. Biol.*, vol. 12, no. 5, May 2016, Art. no. e1004858.

[22] M. I. Rabinovich, P. Varona, A. I. Selverston, and H. D. I. Abarbanel, "Dynamical principles in neuroscience," *Rev. Mod. Phys.*, vol. 78, no. 4, p. 1213, Dec. 2006.

[23] H. Riecke, A. Roxin, S. Madruga, and S. A. Solla, "Multiple attractors, long chaotic transients, and failure in small-world networks of excitable neurons," *Chaos Interdiscipl. J. Nonlinear Sci.*, vol. 17, no. 2, Jun. 2007, Art. no. 026110.

[24] M. Shanahan, "Dynamical complexity in small-world networks of spiking neurons," *Phys. Rev. E, Stat. Phys. Plasmas Fluids Relat. Interdiscip. Top.*, vol. 78, no. 4, Oct. 2008, Art. no. 041924.

[25] S. Song, P. J. Sjöström, M. Reigl, S. Nelson, and D. B. Chklovskii, "Highly nonrandom features of synaptic connectivity in local cortical circuits," *PLoS Biol.*, vol. 3, no. 3, p. e68, Mar. 2005.

[26] S. Lefort, C. Tomm, J.-C. F. Sarria, and C. C. H. Petersen, "The excitatory neuronal network of the C2 barrel column in mouse primary somatosensory cortex," *Neuron*, vol. 61, no. 2, pp. 301–316, Jan. 2009.

[27] D. A. McCormick, "Spontaneous activity: Signal or noise?" *Science*, vol. 285, no. 5427, pp. 541–543, 1999.

[28] J. Fiser, C. Chiu, and M. Weliky, "Small modulation of ongoing cortical dynamics by sensory input during natural vision," *Nature*, vol. 431, no. 7008, pp. 573–578, Sep. 2004.

[29] T. Samura, Y. Ikegaya, and Y. D. Sato, "A neural network model of reliably optimized spike transmission," *Cognit. Neurodynamics*, vol. 9, no. 3, pp. 265–277, Jun. 2015.

[30] J.-N. Teramae, "Long-tailed distribution of synaptic strength reveals origin and functional roles of ongoing fluctuation in cortical circuit," in *Proc. AIP Conf.*, 2016, vol. 1738, no. 1, p. 210016.

[31] B. Kriener, H. Enger, T. Tetzlaff, H. E. Plesser, M.-O. Gewaltig, and G. T. Einevoll, "Dynamics of self-sustained asynchronous-irregular activity in random networks of spiking neurons with strong synapses," *Frontiers Comput. Neurosci.*, vol. 8, p. 136, Oct. 2014.

[32] H. Kada, J.-N. Teramae, and I. T. Tokuda, "Highly heterogeneous excitatory connections require less amount of noise to sustain firing activities in cortical networks," *Frontiers Comput. Neurosci.*, vol. 12, p. 104, Dec. 2018.

[33] S. Nobukawa, H. Nishimura, and T. Yamanishi, "Temporal-specific complexity of spiking patterns in spontaneous activity induced by a dual complex network structure," *Sci. Rep.*, vol. 9, no. 1, pp. 1–12, Dec. 2019.

[34] H. Hirase, X. Leinekugel, A. Czurkó, J. Csicsvari, and G. Buzsáki, "Firing rates of hippocampal neurons were preserved during subsequent sleep episodes and modified by novel awake experience," *Proc. Nat. Acad. Sci. USA*, vol. 98, no. 16, pp. 9386–9390, 2001.

[35] K. Mizuseki and G. Buzsáki, "Preconfigured, skewed distribution of firing rates in the hippocampus and entorhinal cortex," *Cell Rep.*, vol. 4, no. 5, pp. 1010–1021, Sep. 2013.

[36] F. P. Battaglia, G. R. Sutherland, S. L. Cowen, B. L. Mc Naughton, and K. D. Harris, "Firing rate modulation: A simple statistical view of memory trace reactivation," *Neural Netw.*, vol. 18, no. 9, pp. 1280–1291, Nov. 2005.

[37] M. Shafi, Y. Zhou, J. Quintana, C. Chow, J. Fuster, and M. Bodner, "Variability in neuronal activity in primate cortex during working memory tasks," *Neuroscience*, vol. 146, no. 3, pp. 1082–1108, May 2007.

[38] T. Hromádka, M. R. DeWeese, and A. M. Zador, "Sparse representation of sounds in the unanesthetized auditory cortex," *PLoS Biol.*, vol. 6, no. 1, p. e16, Jan. 2008.

[39] D. H. O'Connor, S. P. Peron, D. Huber, and K. Svoboda, "Neural activity in barrel cortex underlying vibrissa-based object localization in mice," *Neuron*, vol. 67, no. 6, pp. 1048–1061, Sep. 2010.

[40] A. Peyrache *et al.*, "Spatiotemporal dynamics of neocortical excitation and inhibition during human sleep," *Proc. Nat. Acad. Sci. USA*, vol. 109, no. 5, pp. 1731–1736, Jan. 2012.

[41] K. Mizuseki and G. Buzsaki, "Theta oscillations decrease spike synchrony in the hippocampus and entorhinal cortex," *Phil. Trans. Roy. Soc. B, Biol. Sci.*, vol. 369, no. 1635, Feb. 2014, Art. no. 20120530.

[42] W. J. M. Levelt, "Note on the distribution of dominance times in binocular rivalry," *Brit. J. Psychol.*, vol. 58, nos. 1–2, pp. 143–145, May 1967.

[43] A. Borsellino, A. Marco, A. Allazetta, S. Rinesi, and B. Bartolini, "Reversal time distribution in the perception of visual ambiguous stimuli," *Kybernetik*, vol. 10, no. 3, pp. 139–144, Mar. 1972.

[44] P. Walker, "Stochastic properties of binocular rivalry alternations," *Perception Psychophysics*, vol. 18, no. 6, pp. 467–473, Nov. 1975.

[45] S. R. Lehky, "Binocular rivalry is not chaotic," *Proc. Roy. Soc. Lond. B, Biol. Sci.*, vol. 259, no. 1354, pp. 71–76, 1995.

[46] R. Blake and N. K. Logothetis, "Visual competition," *Nature Rev. Neurosci.*, vol. 3, no. 1, p. 13, 2002.

[47] F. Y. K. Kossio, S. Goedeke, B. van den Akker, B. Ibarz, and R.-M. Memmesheimer, "Growing critical: Self-organized criticality in a developing neural system," *Phys. Rev. Lett.*, vol. 121, no. 5, Aug. 2018, Art. no. 058301.

[48] N. Nagao, H. Nishimura, and N. Matsui, "A neural chaos model of multistable perception," *Neural Process. Lett.*, vol. 12, no. 3, pp. 267–276, 2000.

[49] T. Kanamaru, "Chaotic pattern alternations can reproduce properties of dominance durations in multistable perception," *Neural Comput.*, vol. 29, no. 6, pp. 1696–1720, Jun. 2017.

[50] D. Martí, N. Brunel, and S. Ostojic, "Correlations between synapses in pairs of neurons slow down dynamics in randomly connected neural networks," *Phys. Rev. E, Stat. Phys. Plasmas Fluids Relat. Interdiscip. Top.*, vol. 97, no. 6, Jun. 2018, Art. no. 062314.

[51] F. Mastrogiuseppe and S. Ostojic, "Intrinsically-generated fluctuating activity in excitatory-inhibitory networks," *PLOS Comput. Biol.*, vol. 13, no. 4, Apr. 2017, Art. no. e1005498.

[52] C. Gilbert and T. Wiesel, "Clustered intrinsic connections in cat visual cortex," *J. Neurosci.*, vol. 3, no. 5, pp. 1116–1133, May 1983.

[53] C. Gilbert and T. Wiesel, "Columnar specificity of intrinsic horizontal and corticocortical connections in cat visual cortex," *J. Neurosci.*, vol. 9, no. 7, pp. 2432–2442, Jul. 1989.

[54] E. M. Callaway and L. C. Katz, "Effects of binocular deprivation on the development of clustered horizontal connections in cat striate cortex," *Proc. Nat. Acad. Sci. USA*, vol. 88, no. 3, pp. 745–749, Feb. 1991.

[55] E. M. Callaway, "Local circuits in primary visual cortex of the macaque monkey," *Annu. Rev. Neurosci.*, vol. 21, no. 1, pp. 47–74, Mar. 1998.

[56] N. Wagatsuma, T. C. Potjans, M. Diesmann, and T. Fukai, "Layer-dependent attentional processing by top-down signals in a visual cortical microcircuit model," *Frontiers Comput. Neurosci.*, vol. 5, p. 31, Jul. 2011.

[57] N. Wagatsuma, T. C. Potjans, M. Diesmann, K. Sakai, and T. Fukai, "Spatial and feature-based attention in a layered cortical microcircuit model," *PLoS ONE*, vol. 8, no. 12, Dec. 2013, Art. no. e80788.

[58] B. Lee, D. Shin, S. P. Gross, and K.-H. Cho, "Combined positive and negative feedback allows modulation of neuronal oscillation frequency during sensory processing," *Cell Rep.*, vol. 25, no. 6, pp. 1548–1560, 2018.

[59] M. Morishima, "Recurrent connection patterns of corticostriatal pyramidal cells in frontal cortex," *J. Neurosci.*, vol. 26, no. 16, pp. 4394–4405, Apr. 2006.

[60] C. R. Gerfen, M. N. Economo, and J. Chandrashekar, "Long distance projections of cortical pyramidal neurons," *J. Neurosci. Res.*, vol. 96, no. 9, pp. 1467–1475, Sep. 2018.

[61] A. N. Burkitt, "A review of the integrate-and-fire neuron model: II. Inhomogeneous synaptic input and network properties," *Biol. Cybern.*, vol. 95, no. 2, pp. 97–112, Aug. 2006.

[62] T. Kanamaru and M. Sekine, "Analysis of globally connected active rotators with excitatory and inhibitory connections using the Fokker-Planck equation," *Phys. Rev. E, Stat. Phys. Plasmas Fluids Relat. Interdiscip. Top.*, vol. 67, no. 3, Mar. 2003, Art. no. 031916.

[63] G. Kovačič, L. Tao, A. V. Rangan, and D. Cai, "Fokker-Planck description of conductance-based integrate-and-fire neuronal networks," *Phys. Rev. E, Stat. Phys. Plasmas Fluids Relat. Interdiscip. Top.*, vol. 80, no. 2, Aug. 2009, Art. no. 021904.

[64] S. Nobukawa, H. Nishimura, and T. Yamanishi, "Skewed and long-tailed distributions of spiking activity in coupled network modules with log-normal synaptic weight distribution," in *Proc. 25th Int. Conf. Neural Inf. Process. (ICONIP)*. Berlin, Germany: Springer, 2018, pp. 535–544.

[65] D. F. Goodman, M. Stimberg, P. Yger, and R. Brette, "Brian 2: Neural simulations on a variety of computational hardware," *BMC Neurosci.*, vol. 15, no. 1, p. P199, 2014.

[66] C. J. Stam, G. Nolte, and A. Daffertshofer, "Phase lag index: Assessment of functional connectivity from multi channel EEG and MEG with diminished bias from common sources," *Human Brain Mapping*, vol. 28, no. 11, pp. 1178–1193, 2007.

[67] T. Takahashi *et al.*, "Band-specific atypical functional connectivity pattern in childhood autism spectrum disorder," *Clin. Neurophysiol.*, vol. 128, no. 8, pp. 1457–1465, Aug. 2017.

[68] T. Takahashi *et al.*, "Abnormal functional connectivity of high-frequency rhythms in drug-naïve schizophrenia," *Clin. Neurophysiol.*, vol. 129, no. 1, pp. 222–231, Jan. 2018.

[69] S. Nobukawa, M. Kikuchi, and T. Takahashi, "Changes in functional connectivity dynamics with aging: A dynamical phase synchronization approach," *NeuroImage*, vol. 188, pp. 357–368, Mar. 2019.

[70] M. Costa, A. L. Goldberger, and C.-K. Peng, "Multiscale entropy analysis of complex physiologic time series," *Phys. Rev. Lett.*, vol. 89, no. 6, Jul. 2002, Art. no. 068102.

[71] T. Schreiber and A. Schmitz, "Improved surrogate data for nonlinearity tests," *Phys. Rev. Lett.*, vol. 77, no. 4, p. 635, 1996.

[72] R. D. Traub, J. G. Jefferys, and M. A. Whittington, *Fast Oscillations Cortical Circuits*. Cambridge, MA, USA: MIT Press, 1999.

[73] M. A. Whittington, R. D. Traub, N. Kopell, B. Ermentrout, and E. H. Buhl, "Inhibition-based rhythms: Experimental and mathematical observations on network dynamics," *Int. J. Psychophysiol.*, vol. 38, no. 3, pp. 315–336, Dec. 2000.

[74] E. M. Izhikevich, "Simple model of spiking neurons," *IEEE Trans. Neural Netw.*, vol. 14, no. 6, pp. 1569–1572, Nov. 2003.

[75] C. Börgers and N. Kopell, "Synchronization in networks of excitatory and inhibitory neurons with sparse, random connectivity," *Neural Comput.*, vol. 15, no. 3, pp. 509–538, Mar. 2003.

[76] M. Bartos, I. Vida, and P. Jonas, "Synaptic mechanisms of synchronized gamma oscillations in inhibitory interneuron networks," *Nature Rev. Neurosci.*, vol. 8, no. 1, pp. 45–56, Jan. 2007.

[77] A. Hasenstaub, Y. Shu, B. Haider, U. Kraushaar, A. Duque, and D. A. McCormick, "Inhibitory postsynaptic potentials carry synchronized frequency information in active cortical networks," *Neuron*, vol. 47, no. 3, pp. 423–435, Aug. 2005.

[78] G. T. Neske and B. W. Connors, "Synchronized gamma-frequency inhibition in neocortex depends on excitatory-inhibitory interactions but not electrical synapses," *J. Neurophysiol.*, vol. 116, no. 2, pp. 351–368, Aug. 2016.

[79] J. H. Lee, T. Delbruck, and M. Pfeiffer, "Training deep spiking neural networks using backpropagation," *Frontiers Neurosci.*, vol. 10, p. 508, Nov. 2016.

[80] X. Lin, X. Wang, and Z. Hao, "Supervised learning in multilayer spiking neural networks with inner products of spike trains," *Neurocomputing*, vol. 237, pp. 59–70, May 2017.

[81] S. R. Kulkarni and B. Rajendran, "Spiking neural networks for handwritten digit recognition—Supervised learning and network optimization," *Neural Netw.*, vol. 103, pp. 118–127, Jul. 2018.

[82] S. R. Kheradpisheh, M. Ganjtabesh, S. J. Thorpe, and T. Masquelier, "STDP-based spiking deep convolutional neural networks for object recognition," *Neural Netw.*, vol. 99, pp. 56–67, Mar. 2018.

[83] Z. Lin, D. Ma, J. Meng, and L. Chen, "Relative ordering learning in spiking neural network for pattern recognition," *Neurocomputing*, vol. 275, pp. 94–106, Jan. 2018.

[84] A. Tavanaei, T. Masquelier, and A. Maida, "Representation learning using event-based STDP," *Neural Netw.*, vol. 105, pp. 294–303, Sep. 2018.

[85] M. Mozafari, S. R. Kheradpisheh, T. Masquelier, A. Nowzari-Dalini, and M. Ganjtabesh, "First-spike-based visual categorization using reward-modulated STDP," *IEEE Trans. Neural Netw. Learn. Syst.*, vol. 29, no. 12, pp. 6178–6190, Dec. 2018.

[86] A. Tavanaei, Z. Kirby, and A. S. Maida, "Training spiking ConvNets by STDP and gradient descent," in *Proc. Int. Joint Conf. Neural Netw. (IJCNN)*, Jul. 2018, pp. 1–8.

[87] Y. Wu, L. Deng, G. Li, J. Zhu, and L. Shi, "Spatio-temporal backpropagation for training high-performance spiking neural networks," *Frontiers Neurosci.*, vol. 12, p. 331, May 2018.

[88] G. Bellec, D. Salaj, A. Subramoney, R. Legenstein, and W. Maass, "Long short-term memory and learning-to-learn in networks of spiking neurons," in *Advances in Neural Information Processing Systems*, S. Bengio, H. Wallach, H. Larochelle, K. Grauman, N. Cesa-Bianchi, and R. Garnett, Eds. Red Hook, NY, USA: Curran Associates, 2018, pp. 795–805.

[89] N. Hiratani, J.-N. Teramae, and T. Fukai, "Associative memory model with long-tail-distributed Hebbian synaptic connections," *Frontiers Comput. Neurosci.*, vol. 6, p. 102, Feb. 2013.

[90] J. Zhang, Y. Shao, A. V. Rangan, and L. Tao, "A coarse-graining framework for spiking neuronal networks: From strongly-coupled conductance-based integrate-and-fire neurons to augmented systems of ODEs," *J. Comput. Neurosci.*, vol. 46, no. 2, pp. 211–232, Apr. 2019.

[91] R. Gast, H. Schmidt, and T. R. Knösche, "A mean-field description of bursting dynamics in spiking neural networks with short-term adaptation," *Neural Comput.*, vol. 32, no. 9, pp. 1615–1634, 2020.

Sou Nobukawa (Member, IEEE) graduated from the Department of Physics and Earth Sciences, The University of the Ryukyus, Nishihara, Japan, in 2006. He received the Ph.D. degree from the University of Hyogo, Kobe, Japan, in 2013.

He is currently an Associate Professor with the Department of Computer Science, Chiba Institute of Technology, Chiba, Japan. His research interests include chaos/bifurcation and neural networks.

Dr. Nobukawa is also a member of the International Neural Network Society (INNS), the Institute of Electronics, Information and Communication Engineers (IEICE), the Information Processing Society of Japan (IPSJ), the Society of Instrument and Control Engineers (SICE), the Institute of Systems, Control and Information Engineers (ISCIE), and others. He received the SICE Encouraging Prize in 2016, the Young Researcher Award by the IEEE Computational Intelligence Society Japan Chapter, and Best Paper Award of The 29th Symposium on Fuzzy, Artificial Intelligence, Neural Networks and Computational Intelligence in 2019.

Haruhiko Nishimura (Member, IEEE) graduated from the Department of Physics, Shizuoka University, Shizuoka, Japan, in 1980. He received the Ph.D. degree from Kobe University, Kobe, Japan, in 1985.

He is currently a Professor in the Graduate School of Applied Informatics, University of Hyogo, Kobe. His research interests include intelligent systems' science based on several architectures, such as neural networks and complex systems. He is also currently engaged in research in biomedical, healthcare, and high-confidence sciences.

Dr. Nishimura is also a member of the Institute of Electronics, Information and Communication Engineers (IEICE), the Information Processing Society of Japan (IPSJ), the Institute of Systems, Control and Information Engineers (ISCIE), Japanese Neural Network Society (JNNS), and other organizations. He received the ISCIE Paper Prize in 2001 and the JSKE Paper Prize in 2010.

Satoshi Ando graduated from the Department of Computer Science, Chiba Institute of Technology, Chiba, Japan, in 2019.

He is currently an Engineer with JSOL Corporation, Tokyo, Japan. His research interest includes nonlinear dynamics of spiking neural networks.

Nobuhiko Wagatsuma received the B.S., M.S., and Ph.D. degrees from the University of Tsukuba, Tsukuba, Japan, in 2004, 2006, and 2009, respectively.

He is currently a Lecturer with the Department of Information Science, Faculty of Science, Toho University, Chiba, Japan. His research interests include visual attention and computational neuroscience.

Teruya Yamanishi received the master's degree in science education and the Ph.D. degree in physics from Kobe University, Kobe, Japan, in 1991 and 1994, respectively.

He is currently a Professor with the Fukui University of Technology, Fukui, Japan, where he studies mathematical information science for the brain and develops tools to optimize the behavior of autonomous robots.